Engineering Fracture Mechanics 229 (2020) 106929

Contents lists available at ScienceDirect

Engineering Fracture Mechanics

journal homepage: www.elsevier.com/locate/engfracmech

Accessible determination of die-to-wafer bond strength with the Schwickerath test

Shuai Shao[a,*,1], Yuling Niu[a,1], Jing Wang[a,1], Seungbae Park[a], Bongsub Lee[b]

[a] Department of Mechanical Engineering, State University of New York at Binghamton, P.O. Box 6000, Binghamton, NY 13902, USA
[b] Xperi Corporation, 3025 Orchard Pkwy, San Jose, CA 95134, USA

ARTICLE INFO

Keywords:
Direct bonding
Bond energy
Fracture mechanics
Beam theory
Three-point bending test
Finite element method

ABSTRACT

Die-to-wafer or wafer-to-wafer direct bonding has been drawing significant attention and undergoing rapid development for its various applications in three-dimensional integrated circuits (3D-IC), such as image sensors, micro-electro-mechanical system (MEMS) sensors, and stacked memory products. The bond strength is one of the most considerable factors that affect the reliability of such stacked devices. Measurement of wafer-to-wafer bond strength is normally performed by the razor blade method, but there was no such well-established technique for die-to-wafer direct bond. To characterize the die-to-wafer bond strength accurately and conveniently, this work introduced the Schwickerath three-point bending test and derived an analytical solution of bond energy, which does not require initial crack preparation. To examine the correctness of applying this method in a novel area, finite element method (FEM) and razor blade experiments on equivalent samples were conducted. Furthermore, the annealing effect on die-to-wafer bond strength was studied. Top die thickness, loading rate in three-point bending test, and the compensation factor of analytical solution are discussed and summarized in this study.

1. Introduction

For 2.5D and 3D IC technology development, direct bond interconnect technology has become increasingly important as a method to achieve higher I/O density, faster speed and better thermal performance [1]. Compared to thermal compression bonding, die-to-wafer direct bonding is more suitable for high volume production and widespread proliferation of 2.5D and 3D IC packaging [2,3]. With the advantage of being a low-temperature process, it has aroused the interest of researchers and become especially prevalent in many electronic products such as image sensors [4]. After surface polishing and chemical activation, the wafer-to-wafer or die-to-wafer bonding is achieved at room temperature, which is a favorable environmental condition. A low-temperature batch annealing (usually at 150–350 °C) follows the individual stacking. It increases the dielectric-to-dielectric bonding strength and, in case electrical connection is needed, establishes a metal-to-metal connection (commonly Cu-to-Cu) based on the difference in the coefficient of thermal expansion (CTE) between the dielectric and the metal. The direct bonding strength is a principal concern and several reports have put forward methods to analyze it [5–7]. Measurement of wafer-to-wafer bond strength is normally performed by the razor blade method, but there was no such well-established technique for die-to-wafer direct bond.

This work introduces a novel experimental method, Schwickerath test method [8], based on three-point bending of die-to-wafer

* Corresponding author.
E-mail addresses: sshao1@binghamton.edu (S. Shao), yniu1@binghamton.edu (Y. Niu), jwang115@binghamton.edu (J. Wang), sbpark@binghamton.edu (S. Park), bongsub.lee@xperi.com (B. Lee).
[1] These authors equally contributed to this paper.

https://doi.org/10.1016/j.engfracmech.2020.106929
Received 10 November 2019; Received in revised form 8 February 2020; Accepted 10 February 2020
Available online 12 February 2020
0013-7944/

samples. The Schwickerath three-point bending test method laid the foundation of the International Standard ISO 9693:1999 procedure [9]. It was originally developed in the early 1980s after the bonding strength values of multiple bilayer materials were explored, and then it was widely applied for porcelain-to-metal and porcelain-to-zirconia bonding strength determination [8]. On the basis of the Schwickerath test method, Kosyfaki et al. derived and compared the fracture energy method and strain energy release rate method for the subsequent data processing [10]. Through observation of the requirement for evaluation of the adhesion energy, Gee et al. extended the Schwickerath test to glass-ceramic-zirconia bilayer ceramics and showed the feasibility of both three-point bending and four-point bending measurement [11]. Similarly, metal-ceramic bond energy with geometrically simple specimens was investigated using a three-point bending test [12]. The results from Lent et al. demonstrated the reproducibility of the test method as well as the sensitivity to diverse parameters. Inspired by Lenz et al., this study applied the Schwickerath test to a die-to-wafer bond strength measurement with the consideration that single crystal silicon has similar material properties to ceramics [13]. The reference to bond strength characterization and strain energy release rate (SERR) was employed in this work to quantify the bond strength [14,15]. At the same time, the die-to-wafer samples were measured diametrically without initial crack preparation [7]. The fracture crack propagation along the bonding interface in this test demonstrates the accessibility of this method [5].

To validate the three-point test result, the finite element method (FEM) and the razor blade test method were conducted [16–19]. Our recent report [6] showed some initial results based on 3-point bending test, finite element analysis and razor-blade tests. They will be discussed and compared here with the results from additional samples and a newly-derived analytical equation. The razor blade test, also called the double cantilever beam (DCB) technique, is used to measure the work of fracture of bonded interfaces, such as those between silicon wafers [20,21]. A razor blade is carefully inserted between two silicon wafers, guided by their beveled edges, which induces crack propagation along the bond interface [6]. The estimated bonding energy G can be expressed as [22],

$$G = \frac{3\bar{E}_1 t_1^3 \delta^2}{(1 + \alpha\eta^3)L^4}, \tag{1}$$

where $\bar{E}_1$ and t_1 are the top layer modulus and thickness. η is the ratio of the thickness of top part to that of the bottom part, and α is the ratio of the modulus of the top material to that of the bottom material. δ represents the blade thickness. L, the steady-state crack length, is developed at the interface and measured with an infrared camera. Based on the above description, it is evident that inserting a razor blade into a die-to-wafer interface is difficult without such beveled edges. In addition, the thickness of the top die showed great impact on performing this mechanical procedure [7]. We performed the razor blade test on wafer-to-wafer bonding pairs and then mechanically shaped the samples into die-to-wafer forms, on which we could perform the Schwickerath test. The comparison of results validates the procedure developed here. In the aspect of the finite element model, crack tip opening displacement (CTOD) method revealed the relationship between stress intensity factor and the crack tip opening displacement (δ_x and δ_y) at the interface of bilayer materials [23]. With the combination of opening mode and sliding mode, the SERR can be described by the stress intensity factors in two modes [24]. The linear elastic fracture mechanics model conveniently generated the SERR during interfacial delamination [25,26]. Bond energy with different bonding methods, annealing conditions and loading rates are compared and discussed.

2. Methodology

Three methods are presented to determine the bond energy between die and wafer: Schwickerath test followed by analytical solution; finite element analysis; and razor blade measurement. The Schwickerath test utilized three-point-bending method without pre-crack preparation. Then an analytical solution of bond energy was derived based on beam theory and fracture mechanics. In finite element analysis, a fracture model with a minimal virtual initial crack was built and the force data from Schwickerath test were applied as the boundary condition. Then CTOD method was adopted to calculate the crack opening displacements and the bond energy.

2.1. Analytical solution

A 2D three-point bending problem in a two-layer beam structure is shown in Fig. 1. In this work the bottom layer is the silicon substrate and the top layer is the silicon die. A force P is applied to the center of the substrate. Two forces are applied on its both ends,

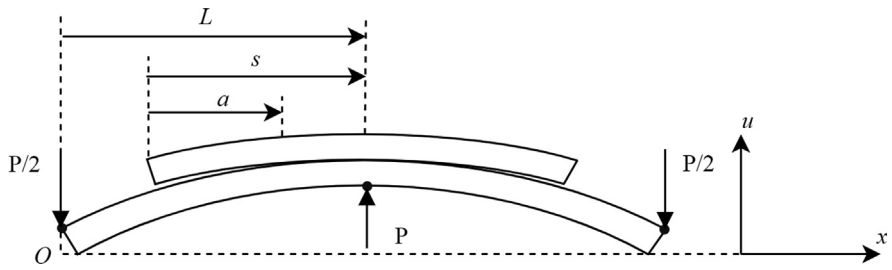

Fig. 1. An illustration of 2D three-point bending problem in a two-layer structure with initial cracks. The length of the initial crack is exaggerated.

which are equal to P/2. Very small initial cracks, with a length of a, are formed at both ends of the top layer. They are exaggerated as plotted in Fig. 1. For linear elastic materials and no residual stress in the sample, the governing equation for the relation between the applied force and the deformation of the sample can be expressed as

$$\frac{d^2u_1}{dx^2} = -\frac{M}{E_sI_s} = -\frac{Px}{2E_sI_s}, \tag{2}$$

$$\frac{d^2u_3}{dx^2} = -\frac{M}{E_cI_c} = -\frac{Px}{2E_cI_c}. \tag{3}$$

where u_1 is the displacement as x is within $(0, \quad L - s + a)$, u_3 is the displacement as x is within $(L - s + a, \quad L)$. Point O is the origin where $x = 0$. L is half length of the total sample. s is half length of the silicon die. I_s is the cross-sectional moment of inertia of the substrate layer, and I_c is the cross-sectional moment of inertia of the dual layer. E_s is the Young's modulus of the substrate layer, and E_c is the Young's modulus of the dual layer.

The boundary conditions in this problem are

$$\frac{du_3}{dx} = 0, \quad \text{at} \quad x = L, \tag{4}$$

$$u_1 = 0, \quad \text{at} \quad x = 0, \tag{5}$$

$$u_1 = u_3, \quad \text{at} \quad x = L - s + a. \tag{6}$$

Eq. (6) is the requirement of displacement continuum at the two cross sections. At $x = L$, the displacement at the load point (center of sample bottom), namely U_3, can be solved as

$$U_3 = u_3|_{x=L} = \frac{P}{6E_cI_c}[L^3 - (L - s + a)^3] + \frac{P}{6E_sI_s}(L - s + a)^3. \tag{7}$$

The detailed derivation process is described in Appendix A. One can see that the displacement is related to applied force, modulus and the geometry.

Based on Howard's work [15], the strain energy release rate G_{ic} available for crack propagation is given by

$$G_{ic} = \frac{P^2}{4b}\left(\frac{dC}{da}\right). \tag{8}$$

where b is the width of the specimen, dC is the change in specimen compliance due to the crack propagation and da is the accompanying change in crack length. Substituting Eq. (7) into Eq. (8) leads to

$$G_{ic} = \frac{P^2}{4b}\left(\frac{dC}{da}\right) = \frac{P^2}{4b}\frac{d}{da}\left(\frac{dU_3}{dP}\right) = \frac{P^2}{8b}\left(\frac{1}{E_sI_s} - \frac{1}{E_cI_c}\right)(L - s + a)^2. \tag{9}$$

As the initial crack a approaches zero, the energy release rate for an intact geometry is obtained.

2.2. Setup of Schwickerath three-point bending test and razor blade test

The purpose of the three-point bending test is to acquire the force-displacement curve and to evaluate die-to-wafer bond energy. Die-to-wafer bonding samples were prepared using the ZiBond® technique [6], which is for direct bonding between dielectric surfaces. We employed thermally oxidized silicon wafers and die, which had 0.5 μm SiO_2 on the surfaces, and performed plasma activation before bonding [6]. In the first case (shown in Fig. 2(a)), actual die-to-wafer bonding was performed. Each die was bonded

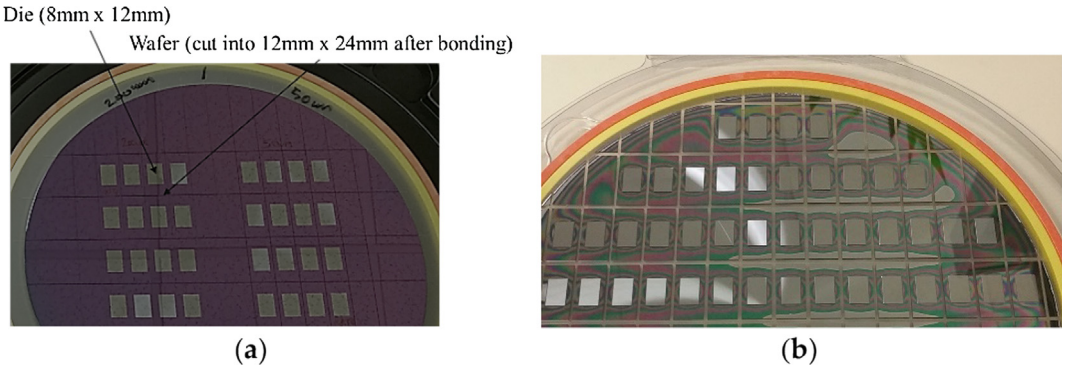

Fig. 2. Image of die-to-wafer samples after bonding, annealing, and wafer cutting: (a) Sample made by true die-to-wafer bonding method employing a pick-and-place machine; (b) Sample originally made by wafer-to-wafer bonding and then shaped into die-to-wafer geometry.

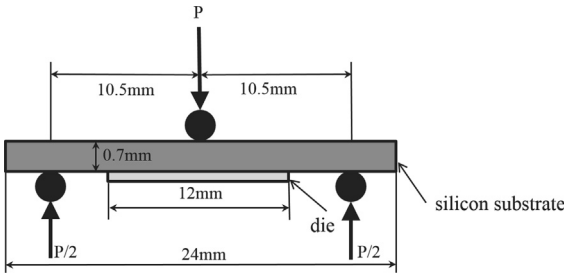

Fig. 3. Illustration of the loading condition of the three-point bending test on the die-on-wafer sample.

to a wafer by a pick-and-place machine at room temperature. After this die-to-wafer bonding was performed on two wafers, one wafer was kept at room temperature and the other was annealed at 150 ˚C for 15 min. The lateral size of the die was 12 mm × 8 mm, and thickness was either 50 μm or 200 μm. This structure reflects a typical design in the actual electronic products. To prepare the sample for mechanical measurements, the wafers were cut into 12 mm × 24 mm strips, which retained the wafer thickness of 700 μm. Note that the width of a wafer strip is larger than the die size, while a previous study [7] had an inconvenient constraint of keeping the die and strip width the same. The die was kept on the center of a wafer strip. In the second case (Fig. 2(b)), we performed wafer-to-wafer bonding and then created the die-to-wafer shape. We bonded two thermally oxidized silicon wafers, annealed the pair, performed razor-blade tests, ground the entire top wafer into a desired thickness, and performed photolithography to make the top wafer into the shape of an array of 12 mm × 8 mm rectangles by patterning and etching the Si. The remaining bottom wafer was cut into 12 mm × 24 mm strips to achieve a die-to-wafer geometry (Fig. 2(b)), equivalent to the first case (Fig. 2(a)). This sample preparation enables the evaluation and comparison of both razor blade test (in the initial wafer-to-wafer configuration) and a three-point bending (in the die-to-wafer configuration). Comparison of the results would validate the three-point bending analysis proposed here. Two different plasma surface activation conditions (“A” or “B”), two annealing conditions (150 ˚C for 15 min or 300 ˚C for 15 min) and three die thicknesses (50 μm, 100 μm, or 200 μm) were tested in this second case. Scanning acoustic microscopy analysis was performed to ensure that there was no void after bonding.

The loading conditions of the test are shown in Fig. 3. The image of the actual test setup is shown in Fig. 4. It is a displacement-control test. The speed of the load (i.e., displacement) is set as low as 0.02 μm/s or 0.05 μm/s.

2.3. Finite element modeling

A 2D finite element facture model of a die on silicon substrate was built using ANSYS. The load conditions of the three-point bending test were applied, as shown in Fig. 5. At the same time, plane-strain condition was adopted. An initial crack in a length of a was modeled along the die-substrate interface at the die edge to perform linear elastic fracture mechanics analysis. A bare silicon substrate strip only was mounted under three-point bending test and the Young’s modulus was obtained as $E = 130$ GPa, which was input as the material property in the FE model. The Poisson’s ratio of silicon is 0.279. The maximum force before it dropped from the test was applied as the boundary condition of the fracture model. The bond energy will be calculated based on the results from finite element analysis later in this paper.

2.4. Calculation of strain energy realease rate (SERR)

The bond energy between die and wafer was released due to interfacial delamination in three-point bending. Calculating SERR during delamination is one of the methods to evaluate bond energy. In this study, the linear elastic fracture mechanics was utilized to characterize die-wafer interfacial delamination. Computational approaches to obtaining SERR results in fracture include virtual crack closure technique (VCCT), crack tip opening displacement method (CTOD) and J-integral method. These methods can be conveniently implemented in the finite element analysis and their SERR results are supposed to be close for brittle material with small scale yielding [25,26].

Crack tip opening displacement (CTOD) method [23] was developed to build the relation between the stress intensity factors and the crack tip opening displacements (δ_x and δ_y) at the bi-material interface. The expression of CTOD for opening mode (Mode I) and

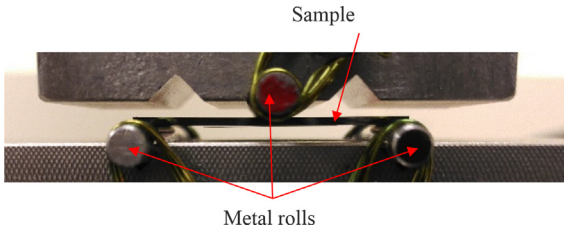

Fig. 4. Image of the sample under load in the three-point bending test.

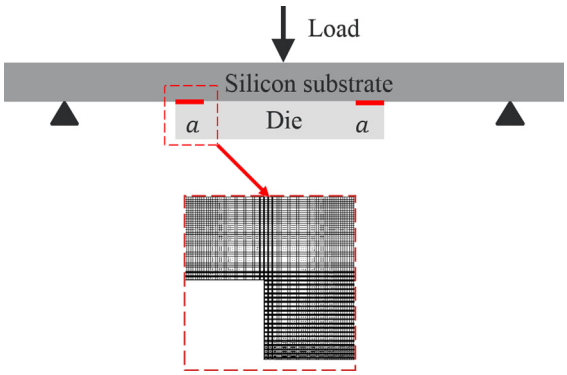

Fig. 5. Illustration of finite element fracture model.

shearing mode (Mode II) is written as

$$\delta_y + i\delta_x = \frac{8}{(1+2i\epsilon)\cosh(\pi\epsilon)}\left(\frac{K_I + iK_{II}}{E^*}\right)\left(\frac{r}{2\pi}\right)^{\frac{1}{2}} r^{i\epsilon} \tag{10}$$

where K_I and K_{II} are stress intensity factors for Mode I and Mode II crack. δ_x and δ_y are crack tip opening displacements in X and Y directions, respectively. r is the distance from the crack tip to the location chosen to acquire the opening displacements. r is typically significantly smaller than the crack opening. E^* is the effective modulus that can be expressed as

$$E^* = \frac{2\bar{E}_1\bar{E}_2}{\bar{E}_1 + \bar{E}_2} \tag{11}$$

where Subscripts 1 and 2 represent two materials. $\bar{E}_i = E_i$ for plane stress condition and $\bar{E}_i = E_i/(1-\nu_i^2)$ for plane strain condition. ϵ is the oscillatory index, which is obtained by

$$\epsilon = \frac{1}{2\pi}\ln\left(\frac{1-\beta_D}{1+\beta_D}\right) \tag{12}$$

where β_D is the Dundurs parameter. β_D is defined as

$$\beta_D = \frac{\mu_1(\kappa_2 - 1) - \mu_2(\kappa_1 - 1)}{\mu_1(\kappa_2 + 1) - \mu_2(\kappa_1 + 1)}, \tag{13}$$

where μ_i is the shear modulus, $\kappa_i = (3-\nu_i)/(1+\nu_i)$in plane stress condition, and $\kappa_i = 3 - 4\nu_i$ in plane strain condition. The physical meaning of E^* and ϵ is understood as the effective material properties adjacent to the crack. K_I and K_{II} can be calculated as follows [24]:

$$K_I = [A\cos(\epsilon \ln r) + B\sin(\epsilon \ln r)]/D, \tag{14}$$

$$K_{II} = [B\cos(\epsilon \ln r) - A\sin(\epsilon \ln r)]/D, \tag{15}$$

where parameters A, B and D are defined as

$$A = \delta_y - 2\epsilon\delta_x, \tag{16}$$

$$B = \delta_x - 2\epsilon\delta_y, \tag{17}$$

$$D = \frac{8}{\cos(\pi\epsilon)}\frac{1}{E^*}\left(\frac{r}{2\pi}\right)^{\frac{1}{2}}. \tag{18}$$

Therefore, the total strain energy release rate G can be obtained by

$$G = \frac{1-\beta_D^2}{E^*}(K_I^2 + K_{II}^2). \tag{19}$$

The phase angle Ψ is obtained by

$$\Psi = \tan^{-1}\left(\frac{K_{II}}{K_I}\right). \tag{20}$$

Eqs. (10)–(20) are used to calculate the energy release rate, or bond energy, G and the phase angle Ψ. Note that acquiring δ_x and δ_y is needed from finite element analysis to apply this method.

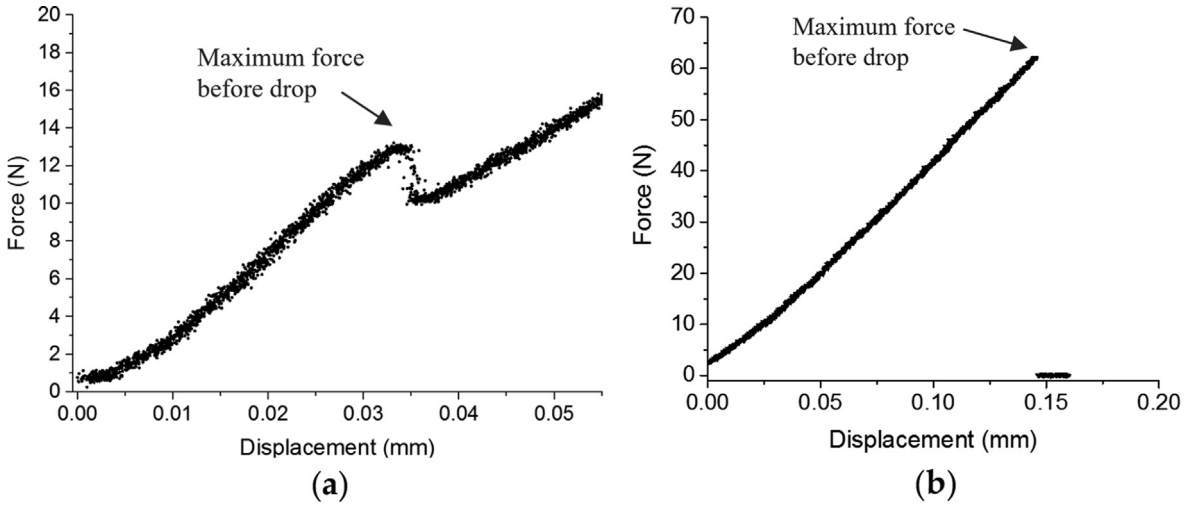

Fig. 6. Force-displacement curves in three-point bending test with die-substrate delamination: (a) Specimen was not annealed. Die thickness is 200 μm; (b) Wafer was annealed at 300 °C for 2 h. Die thickness is 100 μm. Sample broke after the force reached a maximum value. Then the force dropped to zero.

3. Experiment and simulation results

3.1. Experimental results of Schwickerath three-point bending test

The relations between force and displacement are depicted in Fig. 6. The displacement is recorded at the center of substrate where the force was applied. For samples without annealing, the force dropped by a certain amount when delamination occurred and then continued increasing with a smaller amount of slope. The delamination was clearly observed in the test (Fig. 7). For the annealed samples, the force dropped directly to zero after delamination occurred; meanwhile, the sample failed completely. The images of the specimens after failure are shown in Fig. 8. One can see that most area of the die stayed bonded to the silicon substrate. It indicates that the delamination between die and substrate started and stopped near the edge of the die. The maximum value before the force drop occurred was recorded for the subsequent analysis.

The results of maximum force value (before drop) for annealed samples were plotted in Fig. 9, with multiple samples for each die thickness. One can see that the speed of the load (i.e., displacement) did not have much impact on the data, although there is inevitable variation in measured values. This indicates that the speed is low enough and samples reached an equilibrium state during the test.

3.2. Compensation factor on structural compliance

A compensation factor A_{geom} is introduced to address the fact that the silicon substrate and the die have different values of width in the actual samples. By definition, the structural compliance for linear elastic materials is given from Eq. (7) as

$$C = \frac{U_3}{P} = \frac{1}{6E_cI_c}[L^3 - (L - s + a)^3] + \frac{1}{6E_sI_s}(L - s + a)^3. \tag{21}$$

Because the structural compliance changes due to a different geometry, we have

$$A_{geom} = \frac{C^{'}}{C},\ C^{'} = \frac{U_3^{'}}{P^{'}}, \tag{22}$$

where $C^{'}, U_3^{'}, P^{'}$ are the values after compensation, respectively. With $U_3^{'} = U_3$, the bond energy with a compression factor is expressed by,

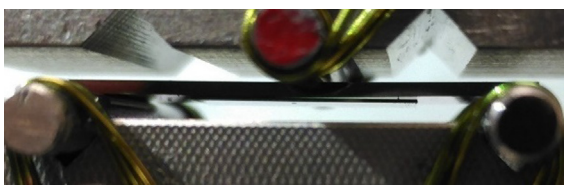

Fig. 7. Delamination of die and silicon substrate was observed during the three-point bending test. The sample was not annealed [6].

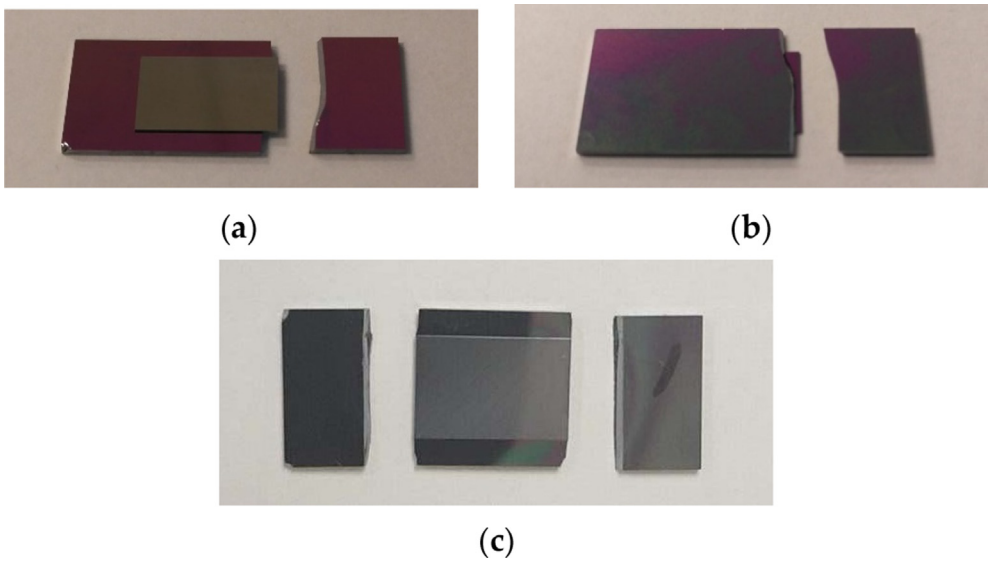

Fig. 8. Images of two annealed samples failed after three-point bending test: (a) Top view of one failed sample; (b) Its bottom view; (c) Another sample failed into three pieces. Most area of the die kept bonded to the silicon substrate.

$$G_{ic}{}' = \frac{G_{ic}}{A_{geom}} = \frac{P^2}{8bA_{geom}}\left(\frac{1}{E_s I_s} - \frac{1}{E_c I_c}\right)(L - s + a)^2. \tag{23}$$

The ratios of compliance between test data and analytical solution for different die thicknesses are listed in Table 1. An averaged value of these is used as the compensation factor $A_{geom} = 1.665$ in this study.

3.3. Finite element analysis and bond energy results

The peak force before drop was used as the force load in the 2D finite element facture model (Fig. 5), because that is the moment when delamination started to initiate. Normal stress contour and shear stress contour around the crack tip are shown in Fig. 10. The normal stress has its direction perpendicular to the crack surface, and the shear stress has its direction parallel to the surface. They correspond to the opening mode and shearing model in fracture. The virtual initial crack is supposed to have a minimal length, so that the calculated bond energy is not sensitive to the value. Also, the mesh density around the crack tip should be high enough to capture the opening displacements accurately. The results of the sensitivity check that address these two aspects are shown in Fig. 11. The variable α in Fig. 11 is defined as the distance between die edge and the supporting metal rolls in the bending test, which is 4.5 mm. $a = \alpha/N$ is the initial crack length in the finite element model, and N the scaling factor to specify the size of the virtual crack length. The crack length becomes smaller as N increases. When $N \geq 250$, the G results become stable (Fig. 11b). A smaller element size means the initial crack length is divided into more elements. The smallest element size in Fig. 11a was used in the finite element model.

Crack tip opening displacements δ_x and δ_y were obtained from the finite element results. Following the CTOD method, bond energy G between die and silicon substrate for each experimental condition was calculated and listed in Table 2. We analyzed seven samples from Wafer #6 and ten samples from all other wafers, then obtained the bond energy values from the average force. The standard deviation of measured force was 14% (Wafer #3) or less. Some CTOD results from Wafers #1–4, 7, 8 were also presented in [6].

4. Discussion

4.1. Delamination of die and silicon substrate

The process of crack propagation during delamination is depicted in Fig. 12. First, the delamination was initiated between the die and the silicon substrate. Then, the delamination did not go further between the die and the silicon substrate because the annealing process made the interface strong. However, micro-cracks were generated on the newly formed surfaces. Finally, the crack path diverted and found a way to continue propagating through the silicon substrate, which caused the sample to break. Ideally this crack propagation happens at the both sides of the sample. Nevertheless, because the loads were not perfectly symmetric on both sides in the test, the failed location was typically on one side. It depends on the margin of error in the asymmetry of fixture design, and the unavoidable difference in the way sample was mounted in the fixture each time.

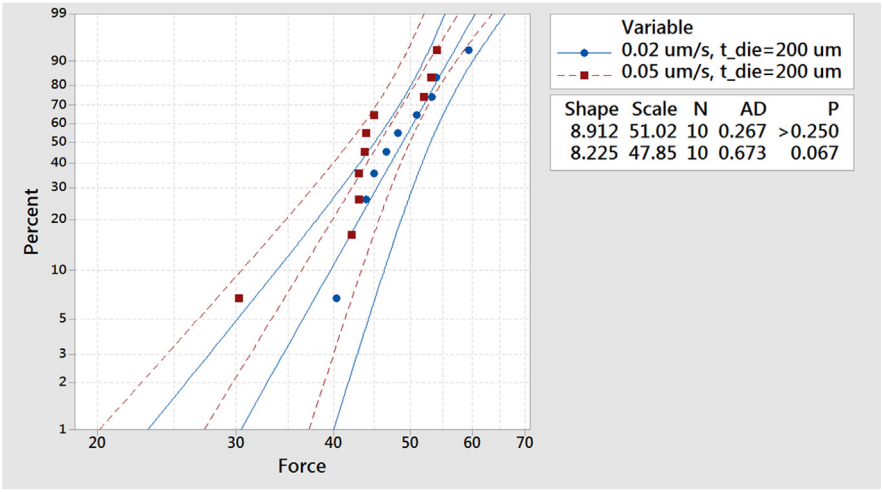

(a)

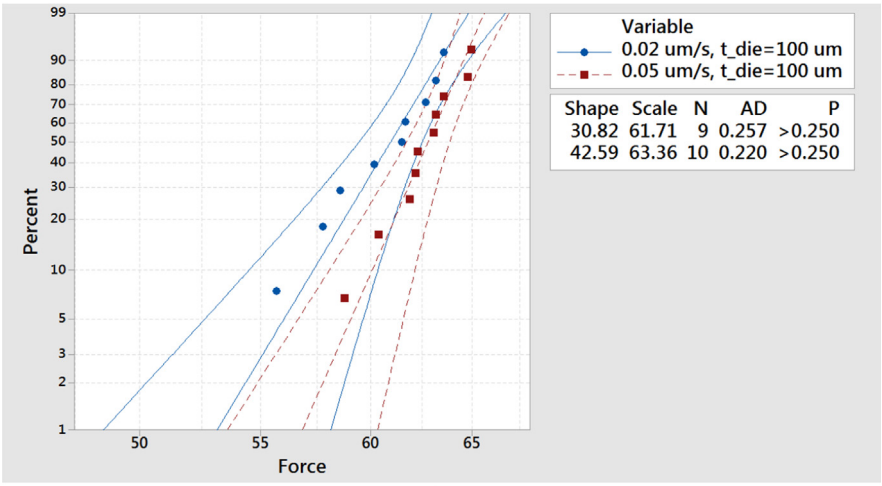

(b)

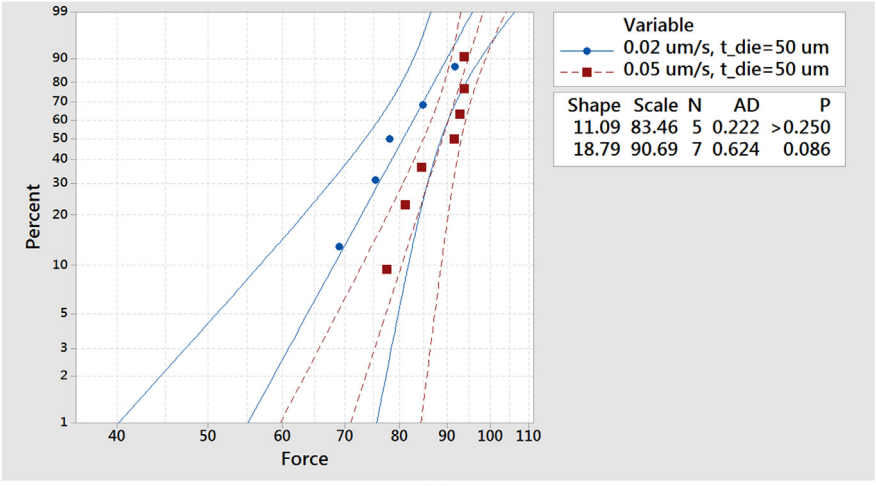

(c)

Fig. 9. Weibull plots of maximum forces for samples with different die thicknesses: (a) die thickness = 200 μm; (b) die thickness = 100 μm; (c) die thickness = 50 μm. All samples were annealed.

Table 1
The compliance of analytical solution and three-point bending test for different die thickness.

Die thickness (μm)	Compliance by analytical solution (mm/N)	Compliance by test (mm/N)	Ratio
200	1.11E − 03	2.17E − 03	1.962
100	1.51E − 03	2.26E − 03	1.499
50	1.79E − 03	2.75E − 03	1.534

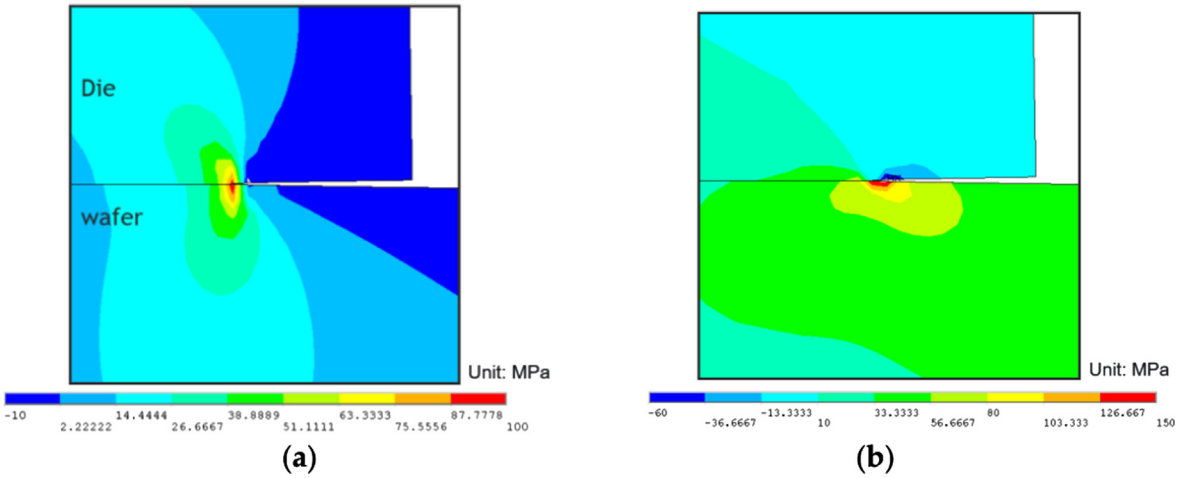

Fig. 10. Stress contour around virtual initial crack between die and silicon substrate: (a) normal stress; (b) shear stress. The deformation is exaggerated.

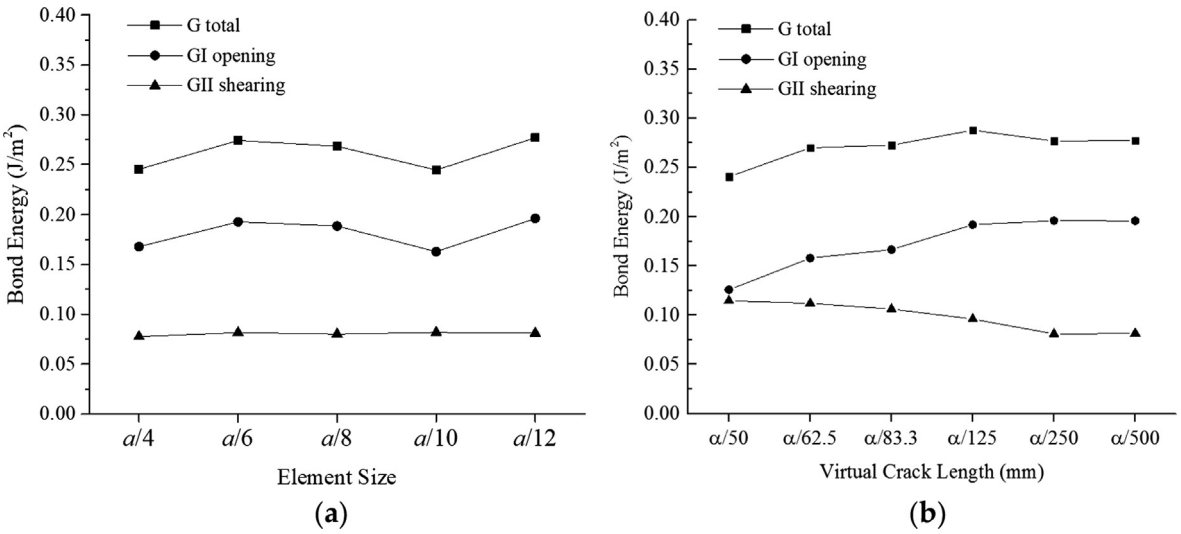

Fig. 11. Sensitive check of finite element modeling: (a) element size around crack tip; (b) initial crack length in the virtual crack technique [6].

4.2. Comparison with 4-point bending test

Four-point bending test is widely used to characterize the bonding property in composite structures. Typically, pre-notched samples are used to precisely control the crack propagation path along the interface between two materials. However, this is highly challenging without making additional damages on the samples under this study. Also, we attempted to use this test method on the samples without preparing initial cracks. Due to the aspect ratio of the samples, they are too short for us to obtain meaningful data in a four-point bending test. The samples always had catastrophic failure under a very high load and did not represent the actual bond energy.

Table 2
Bond energy of samples with different bonding methods, surface activation methods, annealing conditions and die thicknesses.

Wafer	Initial bonding method	Surface activation method	Annealing condition	Die thickness (μm)	Peak force (N)	Bond energy G (J/m^2)
Wafer #1	Pick & place	A	Room Temperature	200	12.8	0.279
Wafer #2	Pick & place	A	Room Temperature	50	26.2	0.282
Wafer #3	Wafer-to-wafer	A	150 °C for 15 min	200	47.9	3.289
Wafer #4	Wafer-to-wafer	A	150 °C for 15 min	200	46.7	3.136
Wafer #5	Wafer-to-wafer	B	300 °C for 2 h	100	61.7	3.228
Wafer #6	Wafer-to-wafer	B	300 °C for 2 h	50	83.5	3.270
Wafer #7	Pick & place	A	150 °C for 15 min	200	26.8	1.142
Wafer #8	Pick & place	A	150 °C for 15 min	50	43.0	0.801

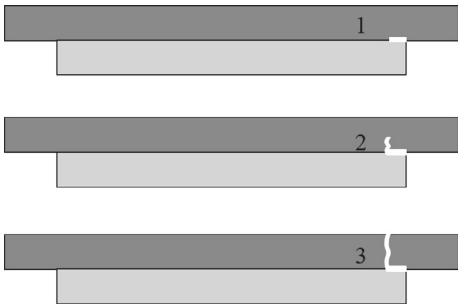

Fig. 12. Illustration of crack propagation before sample failed completely.

4.3. Bond energy obtained from anlytical solution, FEA and razor blade test

The bond energy results from analytical solution, finite element analysis and razor blade test are listed in Table 3. For each wafer, all three methods gave similar results of bond energy as shown in Fig. 13. This indicates the Schwickerath test can be used as a valid method to evaluate die-to-wafer bond energy. Finite element method consistently gives a lower value than the analytical solution does. It is explained by the fact that a finite element model is typically stiffer compared to the calculation based on beam theory. Considering both methods involve the force data from the three-point bending test, a lower structure compliance gives a lower energy bond.

Note that the results from the three methods agree well for each sample, regardless of plasma conditions, annealing conditions and final die thicknesses. For example, bond energy is subjected to the interface quality between wafer and die and supposed to be close among different die thicknesses. Wafer #5 and #6 were produced in the same condition except the final die thickness made by grinding. Indeed, all methods gave very close bond energy data between Wafer #5 and Wafer #6. Therefore, the Schwickerath test is proven as an accessible experiment method to evaluate bond energy between die and wafer. The results it provided fall within an acceptable range of accuracy, which is validated by the results from FEA and razor blade test.

4.4. Repeatability in bond energy assessment

The die-to-wafer bond energy results for Wafer #3 and Wafer #4 in Table 3 are for repeatability check in this study, because they were prepared in the nominally same condition. The reason that analytical solution and FEA results show good repeatability is that the three-point bending test is able to provide consistent force data, which demonstrates the reproducibility of this test method. We observed that razor blade test results are also relatively repeatable as shown between Wafer #5 and Wafer #6, but the results from Wafer #3 and Wafer #4 did not match very well. The reason remains unknown, while one possibility is that the wafer surface condition at the edge could be different in this uncommon case. Note that the razor blade test can only analyze the edge of bonded wafer pairs, while the three-point bending test here does not have such restraint.

Table 3
Bond energy results obtained analytical solution, finite element method, and razor blade measurement.

Wafer	Die thickness (μm)	Analytical solution of bond energy (J/m^2)	Bond energy by FEA (J/m^2)	Razor blade measurement (J/m^2)
Wafer #3	200	3.292	3.289	2.655
Wafer #4	200	3.139	3.136	3.821
Wafer #5	100	3.555	3.228	3.172
Wafer #6	50	3.798	3.270	3.172

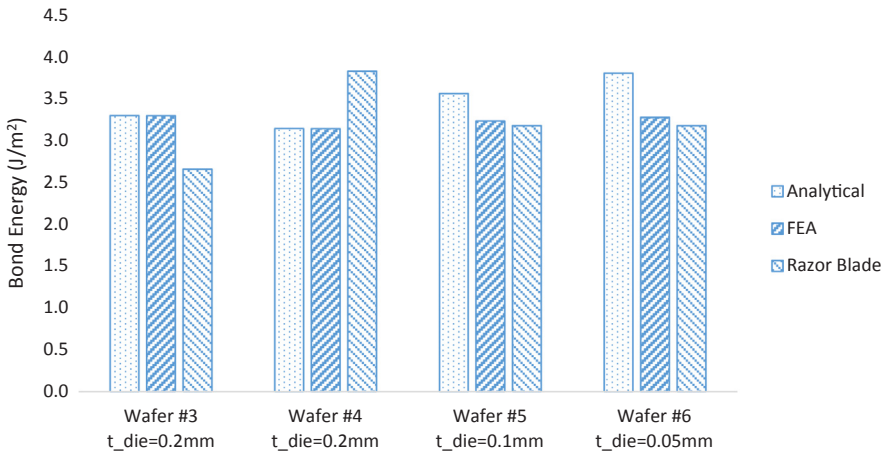

Fig. 13. Comparison of bond energy results from analytical solution, finite element method, and razor blade test.

4.5. Annealing effect on bond energy

Die-to-wafer bond energy with and without annealing are compared in Table 4 and Fig. 14. The samples produced by die-to-wafer bonding (pick-and-place operations) are compared here. Both analytical solutions and FEA results are listed for two die thicknesses. The results show that there is significant difference in bond energy made by the annealing process [6], as well as good agreement between the analytical solution and FEA. The wafers annealed at a higher temperature apparently have a better bonding strength, which is well known for wafer-to-wafer bonding [27]. The mechanism is that the covalent bonds (Si–O–Si) become stronger after annealing. A scratch test, which is often used to evaluate the mechanical adhesion of coatings, was performed for similar die-to-wafer samples and also demonstrated this annealing effect in the previous study [6].

4.6. Effect of bonding process on bond energy

The bond energy data are compared among Wafer #3, #4, #7 and #8 (Table 5). These samples underwent the same surface activation method and the same annealing condition (150 °C), and the only difference was the initial bonding method. The samples from Wafer #3 and Wafer #4 were prepared initially by a wafer-to-wafer bonding process and then shaped into a die-to-wafer-like geometry. For wafer #7 and Wafer #8, an actual die-to-wafer bonding process (pick-and-place operation) was utilized. Compared with a wafer-to-wafer bonding process, a die-to-wafer bonding process typically includes more steps, such as protective coating, die cutting, wet cleaning and pick-and-place operation, which could affect the surface condition and also increase the possibility of introducing particles [6]. In particular, the singulated edges generally have defects which can weaken the bond to the oxide at the die edge. Therefore, the die-to-wafer bonding process (Wafer #7 and Wafer #8) was expected to result in a lower bond energy than the simpler wafer-to-wafer bonding process (Wafer #3 and Wafer #4) [6], as shown in Fig. 15. As discussed in Section 4.3, bond energy does not depend much on the die thickness. There is only a minor difference between the 200 and 50 um thick die and that it is within the tolerance of the measurement.

5. Conclusion

In this paper, the Schwickerath three-point bending test without initial crack preparation is proposed to determine the bond energy resulting from die-to-wafer direct bonding technology. The popular four-point bending test for delamination study did not provide proper results, either because there was great difficulty to prepare an initial crack without damaging the specimen, or because the force required to cause delamination without initial cracks was so high that the specimen had catastrophic failure before delamination occurred. We adopted the Schwickerath three-point bending test inspired by the previous studies on porcelain-to-metal bond characterization and on other brittle materials such as glass. Finite element method (FEM) modeling and razor blade experiments showed good agreement with the analytical solution with an acceptable range of accuracy, proving the validity of this

Table 4
Annealing effect on bond energy by analytical solutions and FEA.

Wafer	Annealing condition	Die thickness (μm)	Bond energy by FEA (J/m^2)	Analytical solution of bond energy (J/m^2)
Wafer #1	Room Temperature	200	0.279	0.246
Wafer #2	Room Temperature	50	0.282	0.364
Wafer #7	150 °C for 15 min	200	1.142	1.079
Wafer #8	150 °C for 15 min	50	0.801	0.981

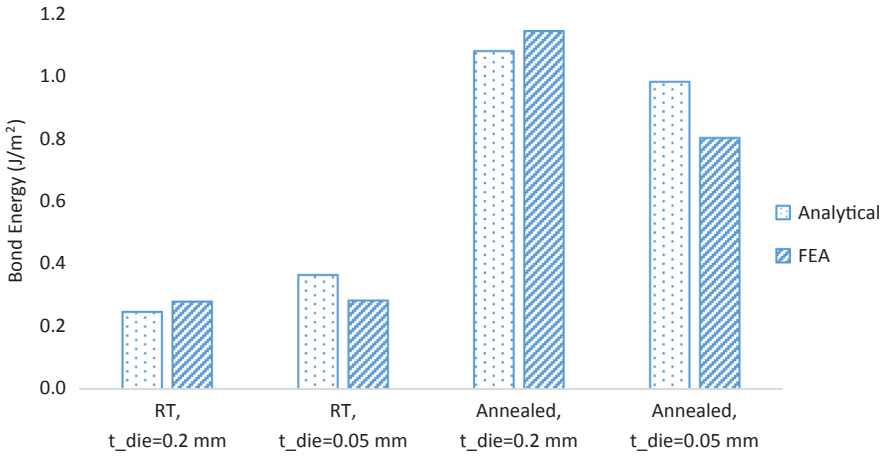

Fig. 14. Bond energy data via analytical solution and finite element analysis for different annealing conditions. RT: Room Temperature.

Table 5
Bond energy obtained by analytical solutions and FEA for different initial bonding methods.

Wafer	Initial bonding method	Die thickness (μm)	Bond energy by FEA (J/m^2)	Analytical solution of bond energy (J/m^2)
Wafer #3	Wafer-to-wafer	200	3.289	3.292
Wafer #4	Wafer-to-wafer	200	3.136	3.139
Wafer #7	Pick & place	200	1.142	1.079
Wafer #8	Pick & place	50	0.801	0.981

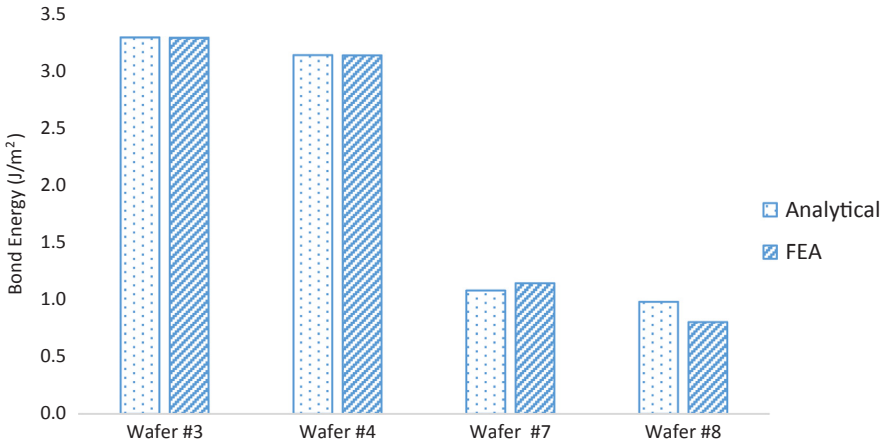

Fig. 15. Bond energy comparison between wafer-to-wafer bonding method and die-to-wafer bonding method via analytical solution and finite element analysis.

Schwickerath method. Furthermore, the annealing effect on die-to-wafer bond strength was studied. High temperature annealing can significantly increase the bond energy and also change the failure mode. Instead of the crack propagating along the interface all the way, it stopped early and diverted its path into the wafer due to its relatively high bond energy. The experimental and simulation results further proved that the top die thickness did not bring a significant influence on the bond energy. Bonding process also made significant difference in bond energy. Die-to-wafer bonding resulted in lower bond energy values than wafer-to-wafer bonding, since a die-to-wafer process typically involves more steps that can affect the interface quality in particular the singulated edges generally have defects which can weaken the bond to the oxide at the die edge. Corroborated by the results from FEA and razor blade tests, the Schwickerath test was validated as an accessible experiment method to quantitatively assess the die-to-wafer bond energy.

Funding

This research received no external funding.

CRediT authorship contribution statement

Shuai Shao: Conceptualization, Methodology, Validation, Formal analysis, Investigation, Resources, Data curation, Writing - original draft, Visualization. **Yuling Niu:** Conceptualization, Methodology, Validation, Formal analysis, Investigation, Resources, Data curation, Writing - original draft, Visualization. **Jing Wang:** Conceptualization, Methodology, Validation, Formal analysis, Investigation, Resources, Data curation, Writing - original draft, Visualization. **Seungbae Park:** Conceptualization, Writing - review & editing, Supervision, Project administration. **Bongsub Lee:** Validation, Resources, Writing - review & editing.

Declaration of Competing Interest

The authors declare that they have no known competing financial interests or personal relationships that could have appeared to influence the work reported in this paper.

Acknowledgements

The authors would like to appreciate all the members of the Opto-Mechanics and Physical Reliability Lab at SUNY-Binghamton for their generous help, and the Invensas team members at Xperi (especially Gill Fountain and Thomas Workman for sample processing and Laura Mirkarimi for technical review).

Appendix A

Solving Eqs. (2) and (3) gives,

$$u_1 = -\frac{Px^3}{12E_sI_s} + c_1x + c_2, \tag{24}$$

$$u_3 = -\frac{Px^3}{12E_cI_c} + c_3x + c_4. \tag{25}$$

Substituting the boundary conditions into the equation above, we have

$$c_3 = \frac{PL^2}{4E_cI_c}, \tag{26}$$

$$c_2 = 0, \tag{27}$$

$$u_1 = -\frac{Px^3}{12E_sI_s} + c_1x, \tag{28}$$

$$u_3 = -\frac{Px^3}{12E_cI_c} + \frac{PL^2x}{4E_cI_c} + c_4, \tag{29}$$

$$c_1 = \frac{P(L-s+a)^2}{4E_sI_s} - \frac{P(L-s+a)^2}{4E_cI_c} + \frac{PL^2}{4E_cI_c}, \tag{30}$$

$$c_4 = \frac{P(L-s+a)^3}{6E_sI_s} - \frac{P(L-s+a)^3}{6E_cE_c}, \tag{31}$$

$$u_3 = -\frac{Px^3}{12E_cI_c} + \frac{PL^2x}{4E_cI_c} + \frac{P(L-s+a)^3}{6E_sI_s} - \frac{P(L-s+a)^3}{6E_cI_c}. \tag{32}$$

References

[1] Gao G, Mirkarimi L, Workman T, Guevara G, Theil J, Uzoh C, et al. Development of low temperature direct bond interconnect technology for die-to-wafer and die-to-die applications – stacking, yield improvement, reliability assessment. In: Proceedings of the 2018 International Wafer Level Packaging Conference (IWLPC). SMTA; 2018. p. 1–7.
[2] Agrawal A, Huang S, Gao G, Wang L, Delacruz J, Mirkarimi L. Thermal and electrical performance of direct bond interconnect technology for 2.5D and 3D integrated circuits. Proceedings of the proceedings of the 2017 IEEE 67th Electronic Components and Technology Conference. 2017. p. 989–98.
[3] Shao S, Liu D, Niu Y, O'Donnell K, Sengupta D, Park SB. A study on the thermomechanical reliability risks of through-silicon-vias in sensor applications. Sensors 2017:17.
[4] Gao G, Mirkarimi L, Fountain G, Wang L, Uzoh C, Workman T, et al. Scaling package interconnects below 20 μm pitch with hybrid bonding. In: Proceedings of the proceedings of the 2018 IEEE 67th electronic components and technology conference. IEEE; 2018. p. 314–322.
[5] Masteika V, Kowal J, Braithwaite NSJ, Rogers T. A review of hydrophilic silicon wafer bonding. J Solid State Sci Technol 2014;3:42–54.
[6] Lee B, Katkar R, Gao G, Lee S, Wang L, Uzoh C, et al. Mechanical strength characterization of direct bond interfaces for 3D-IC and MEMS applications. In: Proceedings of the 2018 IEEE 68th Electronic Components and Technology Conference (ECTC). San Diego, CA: IEEE; 2018. p. 954–961.

[7] Tabata T, Sanchez L, Fournel F, Moriceau H. Reliable four-point flexion test and model for die-to-wafer direct bonding. J Appl Phys 2015;118:015301.
[8] Schneider GA, Swain MV. The Schwickerath adhesion test: A fracture mechanics analysis. Dent Mater 2015;31:986–91.
[9] DIN EN ISO 9693:199(ISO 9693:1999, EN ISO 9693:2000-12); 2012.
[10] Kosyfaki P, Swain MV. Adhesion determination of dental porcelain to zirconia using the Schwickerath test: Strength vs. fracture energy approach. Acta Biomater 2014;10:4861–9.
[11] Gee C, Weddell JN, Swain MV. Comparison of three and four point bending evaluation of two adhesive bonding systems for glass-ceramic zirconia bi-layered ceramics. Dent Mater 2017;33:1004–11.
[12] Lenz J, Schwarz S, Schwickerath H, Sperner F, Schaefer A. Bond strength of metal-ceramic systems in three-point flexure bond test. J Appl Biomater 1995;6:55–64.
[13] Munz D, Fett T. Ceramics: mechanical properties, failure behavior, material selection. Springer; 2001; ISBN 9783642635809.
[14] Gage DM, Kim K, Litteken CS, Dauskardt RH. Role of friction and loading parameters in four-point bend adhesion measurements. J Mater Res 2008;23:87–96.
[15] Howard SJ, Phillipps AJ, Clyne TW. The interpretation of data from the four-point bend delamination test to measure interfacial fracture toughness. Composites 1993;24:103–12.
[16] Matbou Riahi M, Marceau D, Laforte C, Perron J. The experimental/numerical study to predict mechanical behaviour at the ice/aluminium interface. Cold Reg Sci Technol 2011;65:191–202.
[17] Charalambides PG, Lund J, Evans AG, McMeeking RM. A test specimen for determining the fracture resistance of bimaterial interfaces. J Appl Mech 1989;56:77.
[18] Abdelhadi OM, Ladani L, Razmi J. Fracture toughness of bonds using interfacial stresses in four-point bending test. Mech Mater 2011;43:885–900.
[19] Barlow CY, Windle AH. Razor blade test for composite toughness. J Mater Sci Lett 1985;4:233–4.
[20] Maszara WP, Goetz G, Caviglia A, McKitterick JB. Bonding of silicon wafers for silicon-on-insulator. J Appl Phys 1988;64:4943–50.
[21] Kübier JJ. Fracture toughness of ceramics using the SEVNB method: from a preliminary study to a standard test method. Fract Resist Test Monolith Compos Brittle Mater 2002:93–106.
[22] Taylor H, Boning D, Iliescu C. A razor-blade test of the demolding energy in a thermoplastic embossing process. J Micromech Microeng 2011;21:067002.
[23] Suo Z, Hutchinson JW. Interface crack between two elastic layers. Int J Fract 1990;43:1–18.
[24] Ryoji Y, Sang-Bong C. Efficient boundary element analysis of stress intensity factors for interface cracks in dissimilar materials. Eng Fract Mech 1989;34:179–88.
[25] Rice JR. Elastic fracture mechanics concepts for interfacial cracks. J Appl Mech 1988;55:98–103.
[26] Chen X, Lin YCC, Liu X, Lu G-QQ. Fracture mechanics analysis of the effect of substrate flexibility on solder joint reliability. Eng Fract Mech 2005;72:2628–46.
[27] Enquist P. Scalability and low cost of ownership advantages of Direct Bond Interconnect (DBI) as drivers for volume commercialization of 3-D integration architectures and applications. In: Proceedings of the Materials Research Society Fall Meeting; 2008.